geosciences

MDPI

Article

PHOTOSED—PHOTOgrammetric Sediment Erosion Detection

Markus Noack *, Gerhard Schmid, Felix Beckers, Stefan Haun and Silke Wieprecht

Institute for Modelling Hydraulic and Environmental Systems, University of Stuttgart, Pfaffenwaldring 61, 70569 Stuttgart, Germany; gerhard.schmid@iws.uni-stuttgart.de (G.S.); felix.beckers@iws.uni-stuttgart.de (F.B.); stefan.haun@iws.uni-stuttgart.de (S.H.); silke.wieprecht@iws.uni-stuttgart.de (S.W.)

* Correspondence: markus.noack@iws.uni-stuttgart.de; Tel.: +49-711-685-64774

Received: 2 June 2018; Accepted: 29 June 2018; Published: 30 June 2018

Abstract: This work presents a novel high-resolution photogrammetric measuring technique (PHOTOSED) to study in detail the erosion behavior of cohesive sediments, or cohesive/non-cohesive sediment mixtures. PHOTOSED uses a semiconductor laser to project a pseudo-random pattern of light points on a sediment surface and applies the Dense Optical Flow (DOF) algorithm to measure the erosion volume based on displacements of the projected light points during the sediment erosion process. Based on intensive calibration and verification experiments, the accuracy and applicability of the method has been validated for a wide range of erosion volumes, encompassing several orders of magnitude, which is required for investigations of natural sediment mixtures. The high spatial resolution of PHOTOSED is especially designed to detect the substantial variability of erosion rates during exemplary erosion experiments, which allows for further in-depth investigations of the erosion process of cohesive sediments and cohesive/non-cohesive sediment mixtures.

Keywords: cohesive sediments; cohesive/non-cohesive sediment mixtures; erosion behavior; high-spatial resolution measurements; photogrammetric measurements

1. Introduction

The erosion of cohesive sediments and non-cohesive/cohesive sediment mixtures represents a crucial issue for many engineering and ecological applications. Consequently, the erosion behavior has been intensively studied over recent decades in laboratories, as well as in the field. The typical erosion modes for cohesive sediments have been described by several authors in form of particle erosion and the erosion of aggregates (e.g., [1]), which has been extended by Kothyari and Jain [2], and Wu et al. [3] for non-cohesive/cohesive mixtures considering different ratios of cohesive and non-cohesive sediments. Moreover, current scientific literature distinguishes between depth-limited erosion and steady-state erosion [4], dependent on vertical sediment properties. In addition, many efforts have been made to find correlations between critical shear stress, critical velocity, or erosion rates to parameters involved in erosion processes of cohesive sediments, resulting in an immense variety of different formulae (e.g., [3,5–9]). Yet the results of the developed formulae show large differences to each other, are all empirical, and with poor universality [10]. Reasons for these differences are the complex interactions between physical, chemical, and biological parameters (e.g., [11–15]), along with the excessive variety of different devices and methods that were applied to study the erosion process of cohesive sediments [10].

In this context, accurate measurements of erosion rates for cohesive sediment surfaces play an essential role in developing approaches to describe the erosion behavior of non-cohesive/cohesive sediment mixtures. In general, the surface erosion rate is defined as the mass or volume of eroded sediments per surface area and time [16] and is commonly related to the exposed flow conditions

(e.g., as excess shear stress [9]). Aberle et al. [17] have provided an extended overview of different measuring techniques to obtain erosional characteristics of cohesive sediments in the laboratory and field. This review includes recirculating flumes (e.g., [18,19]), straight flow-through flumes (e.g., [20–22]), and miscellaneous devices, such as jet tests (e.g., CSM, cohesive strength meter, Paterson, 1989), hole erosion tests [23], microcosm experiments [24], and erosion bells [25].

Despite the considerable variety of devices, information about the spatial and temporal variability of erosion rates and the capability of the devices to resolve the spatial and temporal variability is rare in literature. Most often, the erosion rates are determined for larger areas, such as the entire surfaces of sediment cores, or the dimensions of open-bottom measuring sections (e.g., [20,21,26]). However, the surface erosion process of cohesive sediments, or non-cohesive/cohesive mixtures, is not homogeneously distributed over the measuring areas. Instead, it shows a high spatial and temporal heterogeneity during the erosion experiments, resulting in a strong structured surface [2]. In addition, the surface evolution to structured surfaces due to erosion leads to different local roughness changes, which affects the local hydraulics and shear stresses, and thus the further progression of erosion. Therefore, this article introduces a novel laboratory method called PHOTOSED (PHOTOgrammetric Sediment Erosion Detection), for the high-resolution measurements of erosion rates from cohesive sediments and non-cohesive/cohesive sediment mixtures using a photogrammetric approach.

2. Materials and Methods

2.1. Experiments in the Erosion Flume—SETEG

The PHOTOSED method was developed for the SETEG-flume (Stroemungskanal zur Ermittlung der tiefenabhängigen Erosionsstabilitaet von Gewaessersedimenten; [22,26,27], Figure 1), which is in use at the Institute for Modelling Hydraulic and Environmental Systems, of the University of Stuttgart, for measuring depth-oriented erosion rates and critical shear stresses for nearly 20 years. The flume (with a height: 0.090 m, width: 0.142 m, and length: 8.320 m) consists of a closed rectangular channel with pressurized flow to obtain optical access for photogrammetric measurements. The measuring section consists of a circular opening in the bottom of the flume where cylindrical sediment cores, with a maximum diameter of 135 mm, can be inserted and are exposed to the fully developed flow. A jack-stepping motor controls vertical movement of the sediments in the core to ensure that the sediment surface is flush with the flume bottom. This arrangement allows for different depths of the sediment core to be investigated independently to obtain depth-oriented information about the erosion behavior. During an erosion experiment, the discharge is increased stepwise until the entrainment of sediment particles, or aggregates, can be observed. The resulting critical shear stress is determined by a hydraulic calibration function (Q-τ-relation), which was obtained by previously conducted high-resolution LDA measurements (TSI Inc., Shoreview, MN, USA). To obtain vertical profiles along the cores, the measurements are typically conducted at depth intervals of 10 mm to 50 mm.

2.2. PHOTOSED—PHOTOgrammetric SEDiment Erosion Detection

For the photogrammetric detection of sediment erosion (PHOTOSED), the SETEG-flume is equipped with a semiconductor laser, with a diffraction optic (Laser2000 GmbH, Wessling, Germany) at the light source, to project a pseudo-random pattern of approximately 24,000 light points on the 143 cm^2 sediment surface (based on the maximum diameter of a sediment core). In addition, a CMOS-camera (2 MP, IDS GmbH, Ettlingen, Germany) is installed for image acquisition, with a temporal resolution of 10 Hz. The laser is mounted outside the flume, and projects down onto the sediment surface in the direction of flow at an angle of 45°, while the CMOS-camera is mounted vertically above the sediment surface. An adjustable pump and magnetic inductive flow-meter (MID) control the flow within the SETEG-flume. Figure 1 shows a schematic overview of the SETEG-flume with the photogrammetric measuring setup.

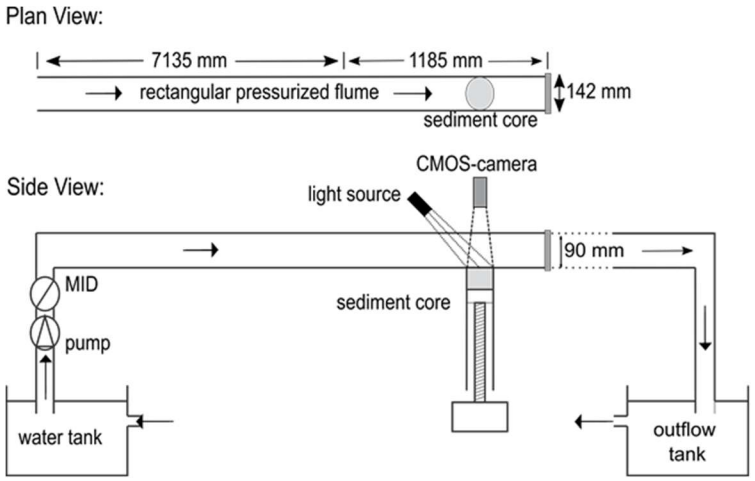

Figure 1. Schematic overview of the SETEG-flume including the experimental setup of PHOTOSED to measure high-resolution erosion rates of cohesive sediments (modified from [22,26,27]).

The measurement of erosion volumes for determining erosion rates considers both bed and suspended load. This represents an advantage compared to devices that determine the erosion rate based solely on suspended load measurements. Several studies showed that bed load could contribute significantly to total erosion [6,13,28]. Within the SETEG-flume, the detection of erosion rates is based on measured erosion volumes in specific time intervals, which depend on the temporal resolution of the CMOS-camera but also on the minimal detectable erosion volume.

PHOTOSED analyzes the displacement of the projected light points for consecutive time-steps that are extracted from continuous image acquisitions of the CMOS-camera. Therefore, an ROI (Region Of Interest) is specified, encompassing a rectangle with a maximum area of 10,426 mm^2 (1600 × 1300 px), to focus on the center of the circular sediment surface and to minimize boundary effects, such as potential erosions at the transition zones between the sediment surface and the flume bottom. To assess the erosion volume between two consecutive images, a Dense Optical Flow (DOF) algorithm of the OpenCV library (Open Source Computer Vision, OpenCV 2.4.10) is used to evaluate the displacements of the projected light points during the erosion process. In contrast to the method of Lucas and Kanade [29], who used the Lagrange tracking method for optical flow assessment to obtain the movement of certain specific pixels (also known as sparse optical flow), the DOF method, developed by Farnebäck [30], is applied. The DOF method is based on a Eulerian approach considering the potential displacement of all pixels between two consecutive images. Therefore, the algorithm searches for identical features between two consecutive images and within a neighborhood of each pixel to approximate the displacements by a polynomial expansion function. The coefficients of the polynomial function are estimated from a weighted least squares fit to the features of the neighboring block. The scale of the block determines the features to which the algorithm is sensitive. A small displacement of the image portions (blocks) can analytically be determined by changing the coefficients of the polynomial expansion at each pixel. For large displacements, the Farnebäck-algorithm is applied on several image pyramid levels to convert the initial large movement into a detectable movement. To use the Farnebäck-algorithm for erosion experiments, the projected random light points are required to provide image features, which are only related to the local surface position, because erosion may result in the image features continuously changing between two consecutive images. The DOF algorithm is implemented into a Python script (version 2.7.8) for the calculation of the erosion volume by using neighboring blocks that are represented by approximately 35 pixels (based on previous investigations with sizes between 15 px and 70 px). The erosion rates are subsequently calculated by considering the time interval between two consecutive images.

2.3. Calibration and Verification Method

To apply photogrammetric approaches for the assessment of erosion volumes using the proposed setup, an in-depth calibration process is required. This must be done to mitigate the optical distortion due to the different refraction indices of the penetrated media (air, water, and glass) and different optical paths between the observed sediment surface and the camera sensor for all pixels. To this end, a calibration setup was developed consisting of a round panel with three circular test areas of different sizes and known geometry. Screws allow for the precise adjustment of the height in the test area, with a full rotation corresponding to a height adjustment of 0.5 mm. To determine the optical distortion, the test areas were vertically shifted for known lengths resulting in known volumes compared to the planar situation. To cover the whole ROI during the calibration process, the test panel was mounted in four different orientations. With this setup, 2D-polynomial correction functions can be determined to account for the optical distortion in x, y, and z-direction and to convert the results from pixel to metric scale.

Figure 2A shows an image of the CMOS-camera including the round panel with the three different test areas, the projected light points, and the ROI. Figure 2B–D exemplary represents a visualization of the DOF algorithm for each test area. For all experiments the camera properties were identical (focal distance: 6.0 mm, aperture: 8, shutter speed: 100–300 ms according to the reflectivity of the sediment surface).

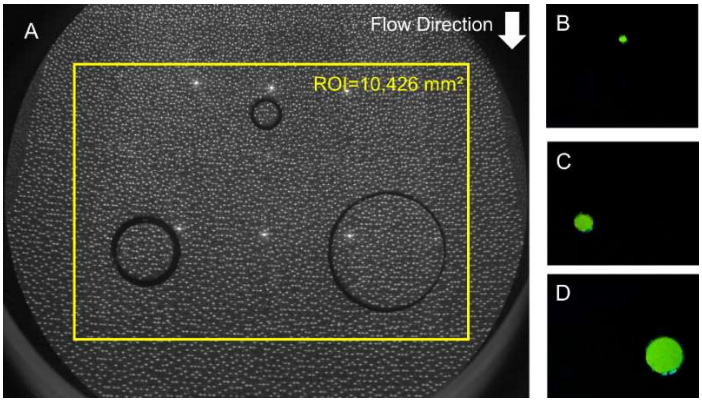

Figure 2. Image of the CMOS-camera showing the round panel of the calibration setup with three different test areas (**A**). Exemplary visualization of the DOF algorithm for each test area, the color represents the drop of the test areas (**B**–**D**).

The projected light pattern in Figure 2A is not uniformly distributed over the ROI due to the angled mounting of the semiconductor laser. This results in a higher point density in the upper part of the ROI and a lower point density in the lower part of the ROI. However, given the high total number of projected points (24,000), the influence on the spatial resolution is only marginal. One projected light point corresponds to 3–6 pixel in diameter depending on the position of the light point. However, the size in pixels for each projected light point is not affecting the accuracy of PHOTOSED because the DOF algorithm detects the displacement of characteristic patterns that consist of several light points. The exemplary visualization of the results of the DOF algorithm (Figure 2B–D) represents the spatial detection of elevation changes for the three different test areas with respect to their initial elevation level. Especially at the edges of the test areas, some imprecise detections can be observed because high gradients of elevation changes may cause erroneous displacement calculations. This impreciseness is also influenced by the chosen block size for the DOF algorithm of 35 px. However, previous investigations showed that a larger block size would degrade the spatial detection for small areas, and a smaller block size would result in a higher noise due to erroneous detections and in a limitation for detecting high surface gradients. For the calibration and

verification of PHOTOSED, the test areas were shifted vertically, which represents in this context a worst-case scenario.

3. Results and Discussion

3.1. Calibration and Verification

To determine the calibration factors in *x*-, *y*- and *z*-direction due to the optical distortion, the three test areas of the calibration panel were stepwise decreased, and the positions were photogrammetrically recorded. To account for different vertical positions, seven positions were measured at a step interval of dz = 0.5 mm. In a second calibration, four vertical positions were measured at a step interval of dz = 1.0 mm. In addition, the orientation of the calibration panel was changed four times to test the influence of the non-uniformly projected light pattern. In total, this calibration concept resulted in 84 different measurements for dz = 0.5 mm (seven vertical positions) and 48 measurements for dz = 1.0 mm (four vertical positions).

For the longitudinal and lateral directions (*x*- and *y*-component), the distortion is nearly symmetrical because of the centered vertical mounting of the camera above the ROI. The mean calibration factor in *x*-direction is dx = 69.2 µm/px, with a standard deviation of σ_x = 0.9 µm/px, while in the *y*-direction the mean calibration factor yields dy = 69.6 µm/px and a standard deviation of σ_y = 1.49 µm/px. Given the symmetry, an equal calibration factor of 69.4 µm/px, with the standard deviation of σ_{xy} = 1.25 µm/px, was chosen for the following procedure.

For the correction in *z*-direction, a 2D-polynomial function is required because of the angled mounting of the semiconductor laser. Figure 3 shows the spatial variation of the calibration factor in *z*-direction for the entire ROI.

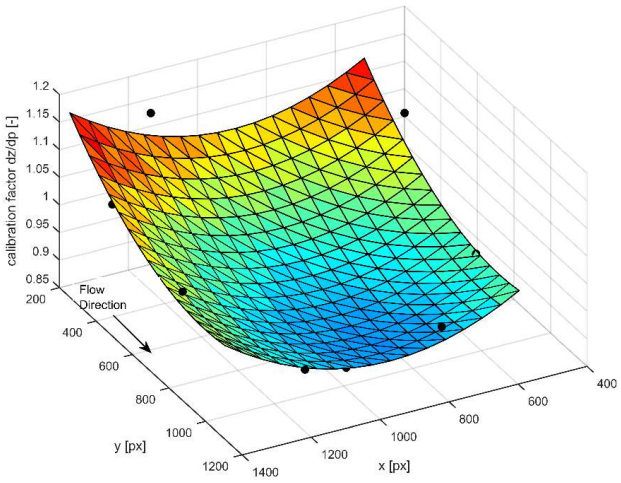

Figure 3. Calibration factor for the vertical scaling from pixel into metric scale of the distorted camera images. The plotted points (n = 12) represent the measurements while the mesh represents their spatial interpolation.

The mean calibration factor in *z*-direction is dz = 111.5 µm/px with a standard deviation of σ_z = 10.3 µm. This calibration factor needs to be multiplied with the position-dependent correction factors in Figure 3 to obtain the correct displacement in the *z*-direction.

3.2. Accuracy of PHOTOSED

Figure 4 represents the measuring accuracy after an incremental shift of the three different test areas of dz = 0.5 mm (Figure 4A) and dz = 1.0 mm (Figure 4B).

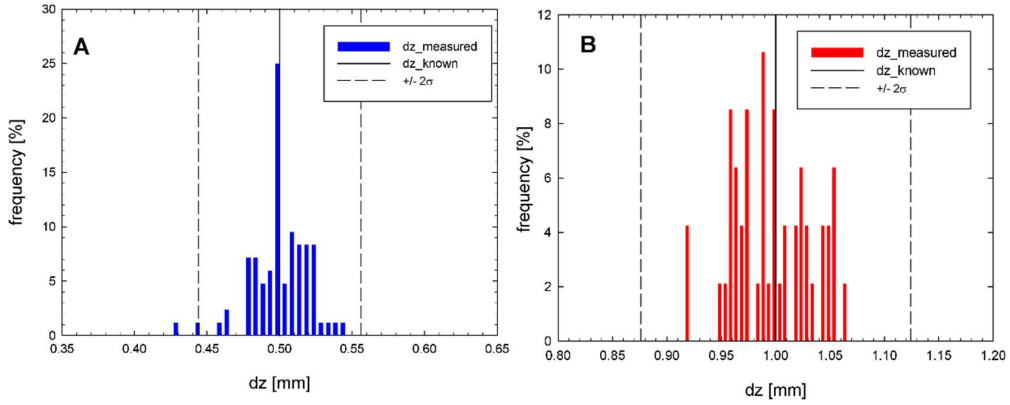

Figure 4. Vertical measuring accuracy of PHOTOSED for given incremental vertical shifts of dz = 0.5 mm (**A**) and dz = 1.0 mm (**B**). The dashed lines represent the median ± the doubled standard deviation (± 2σ).

For Figure 4A, a total of 84 measuring values were evaluated against the known vertical incremental shift of dz = 0.5 mm (in seven vertical positions). 95.45% of all values (2σ) show a deviation of less than 0.028 mm. In Figure 4B, a total of 48 measuring points were evaluated for an incremental shift of dz = 1.0 mm (in four vertical positions) leading to a doubled standard deviation of 2σ = 0.062 mm. Although the doubled standard deviation for a vertical incremental shift of dz = 1.0 mm is higher compared to the vertical shift of dz = 0.5 mm indicating a higher scattering of the obtained data, the relative accuracy (dz/2σ) remains constant. Hence, only the absolute accuracy is affected. The higher scattering results from the angled mounting of the semiconductor laser leading to obscuring and hiding effects regarding projected light points at the boundaries of the displaced area. This effect becomes larger for more pronounced erosion depths. However, the occurred erosion depth between two consecutive images for investigations on sediment surfaces can be subdivided into intermediate stages by shortening the time interval between the two consecutive images given the high temporal resolution of the CMOS-camera (10 Hz).

These measuring results prove the applicability of PHOTOSED for highly accurate measurements of vertical changes based on the DOF algorithm and the applied calibration method.

Figure 5 illustrates the comparison between all predefined and measured volumes with PHOTOSED over several orders of magnitude.

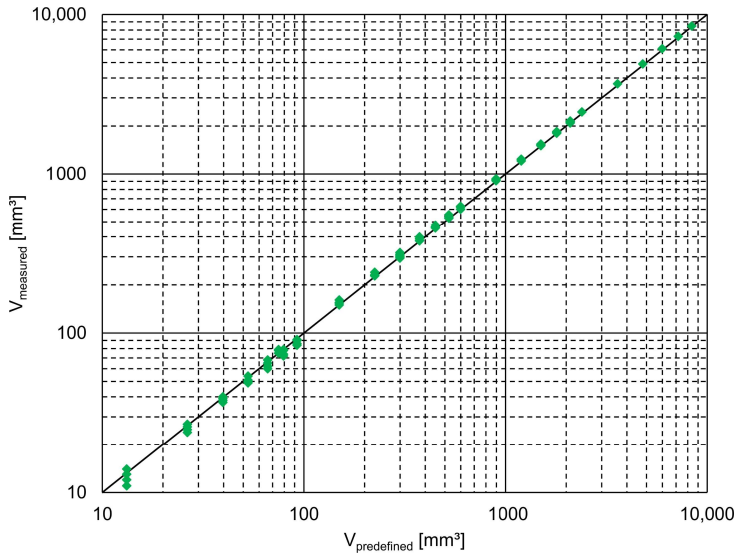

Figure 5. Comparison between photogrammetrically determined volumes against predefined volumes using the three different test areas.

Figure 5 demonstrates the applicability of PHOTOSED for volumes comprising several orders of magnitude ranging from 13 to 8476 mm^3. The mean absolute deviation between photogrammetrically determined volumes to the predefined volumes is 3.24%.

Figure 5 also indicates the lower limits and minimal detectable erosion volumes. For the lowest investigated volume of V = 13 mm^3, the mean absolute deviation reaches a maximum value of 9.2%. This lower detection limit is a result of the point density of the projected light pattern and the required specification of the block size for the DOF algorithm (35 px). The DOF algorithm requires several projected light points for a correct pattern detection; hence, the spatial resolution depends directly on the density of the projected light points. This is predominantly affecting the accuracy on the edges of surface changes. Accordingly, the larger the edges are in comparison to the surface size, the higher the inaccuracy, resulting in a lower detection limit.

Since the erosion of cohesive sediments is highly dynamic and complex, it is often described as a stochastic process given the turbulent nature of flow (e.g., [8]), and the immense number of involved parameters and processes (e.g., [10,11]). The resulting erosion rates can easily vary by several orders of magnitude for the same flow rates [9,26,31]. In this context, the developed photogrammetric method PHOTOSED represents a novel and high-resolution measuring concept to resolve this huge variability of erosion rates for cohesive sediments and offers a wide range of opportunities to perform in-depth investigations of the erosion phenomena of cohesive sediments, or non-cohesive/cohesive sediment mixtures.

3.3. Exemplary Erosion Experiments

After the successful calibration and verification of PHOTOSED, two erosion experiments for one sediment surface, consisting of a cohesive/non-cohesive mixture and two different flow conditions (Q_1 = 7.5 L/s, Q_2 = 11.3 L/s), were conducted to demonstrate the spatial resolution of the photogrammetric approach and to show the spatial and temporal heterogeneity of the measured erosion rates. The particle size distribution of the sediment surface consisted of 8% clay, 83% silt and 9% sand, while the wet bulk density was 1.42 g/cm^3. The flow rates correspond to Reynolds shear stresses of 0.7 Pa (Re = 64,500) and 1.3 Pa (Re = 97,400), respectively. The sediment surface was exposed to the two flow rates for a total time of 600 s each and consecutive images were captured in a temporal resolution of 1.0 s. Figure 6 shows three dimensional plots of the sediment surface at the end of both erosion experiments (t = 600 s) for a flow of Q_1 = 7.5 L/s and Q_2 = 11.3 L/s, respectively.

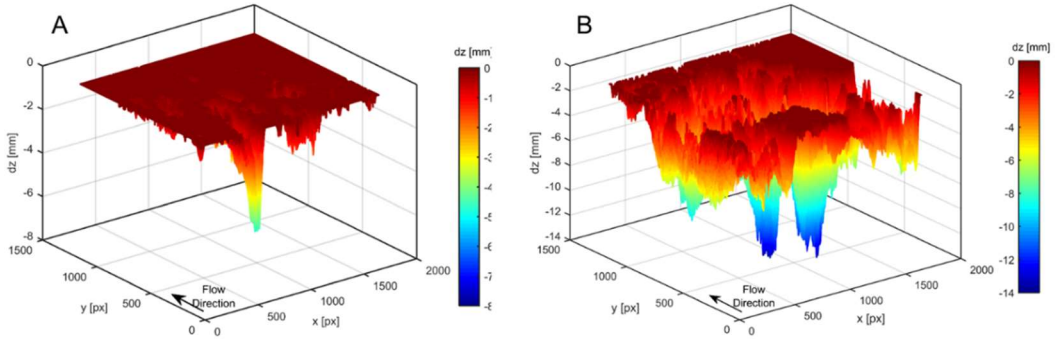

Figure 6. Three-dimensional plots of the sediment surfaces at the end of the erosion experiments after t = 600 s for Q_1 = 7.5 L/s (**A**) and Q_2 = 11.3 L/s (**B**).

The heterogeneity of the occurred erosion is clearly visible for both erosion experiments. For a discharge of Q_1 = 7.5 L/s (Figure 6A) one erosion peak located at the edge of the ROI is observed, indicating a large local erosion. The surrounding smaller erosion peaks are presumably a result of the adjacent erosion peak at the edge of the ROI, which leads to local changes in the topography and roughness. Other areas of the ROI are not eroded at all. For Q_2 = 11.3 L/s (Figure 6B) the erosion is further

developed, showing a second peak with large erosion and a spatial distribution of medium erosion. However, some areas of the surface remain stable without any erosion. Moreover, it becomes obvious that the roughness of such a structured surface will change compared to the initial surface and, consequently, the local shear stresses to which the sediments are exposed to during the erosion experiment.

To quantify the variability of erosion rates of the sediment surface over time, during both erosion experiments, box plots are derived for each pixel ($n = 1.9 \times 10^6$) showing the erosion rates for time intervals of 30 s (Figure 7).

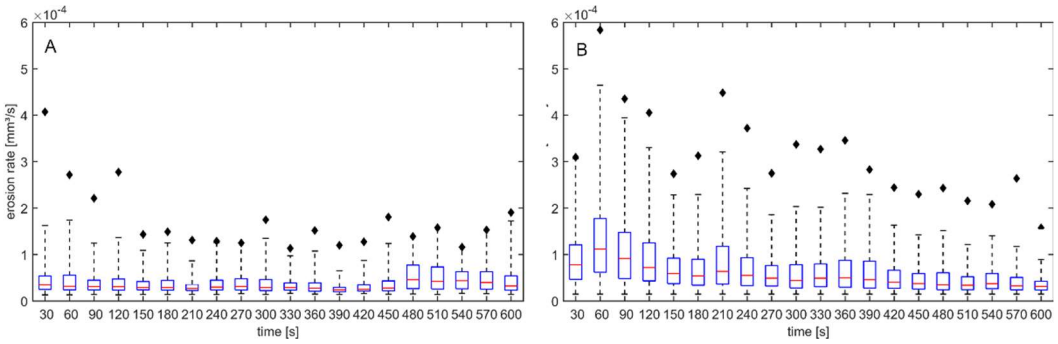

Figure 7. Variability of erosion rates for time intervals of t = 30 s throughout the entire erosion experiments for Q_1 = 7.5 L/s (**A**) and Q_2 = 11.3 L/s (**B**).

In the box plots of Figure 7, the red line for each time-step represents the median value of erosion rates while the bottom and top edges indicate the interquartile range (25th and 75th percentiles) and the whiskers extend to 99.9th percentiles. The filled diamonds represent the maximum measured erosion rate per each time interval of 30 s. For the erosion experiment with Q_1 = 7.5 L/s (Figure 7A), the median of the erosion rates varies between 0.24×10^{-4} mm^3/s and 0.46×10^{-4} mm^3/s, which represents almost a factor of two. The maximum value yields 4.1×10^{-4} mm^3/s during the beginning of the experiment at t = 30 s, when the sediments are first exposed to the flow. However, parts of the sediment surface show no erosion at all. The variability of the erosion rates within each time interval is even higher. Therefore, the median is compared to the maximum values as a criterion for the degree of variability, leading to factors from 2.7 (minimum at t = 540 s) to 11 (maximum at t = 30 s), with a mean value of 5.6, which indicates an extremely high heterogeneity of the obtained erosion rates.

The erosion experiment with Q_2 = 11.3 L/s (Figure 7B) shows, as expected, higher erosion rates with median values ranging from 0.31×10^{-4} to 1.12×10^{-4} mm^3/s. The maximum value for the entire experimental duration is 5.84×10^{-4} mm^3/s (t = 60 s). The minimum variability within one time interval results in a factor of 4.0 at t = 30 s, while the maximum variability yields a factor of 8.1 at t = 570 s. The mean variability yields a value of 6.1 and is slightly higher compared to the erosion experiment with Q_1 = 7.5 L/s.

Both erosion experiments show a high spatial heterogeneity regarding the measured erosion rates. Moreover, it proves that the peak erosion rates occur only very locally (outside the 99.9th percentile) emphasizing the need for high-resolution measurements of erosion rates.

Another strength of PHOTOSED with its high-resolution measurements is the feasibility for detailed investigations of the temporal erosion progress and the eventual formation of erosion patterns over time.

Figure 8A–F show the erosion progress (x-y-plane) for six selected time-steps (Δt = 100 s) of the erosion experiment with a flow rate of Q_2 = 11.3 L/s.

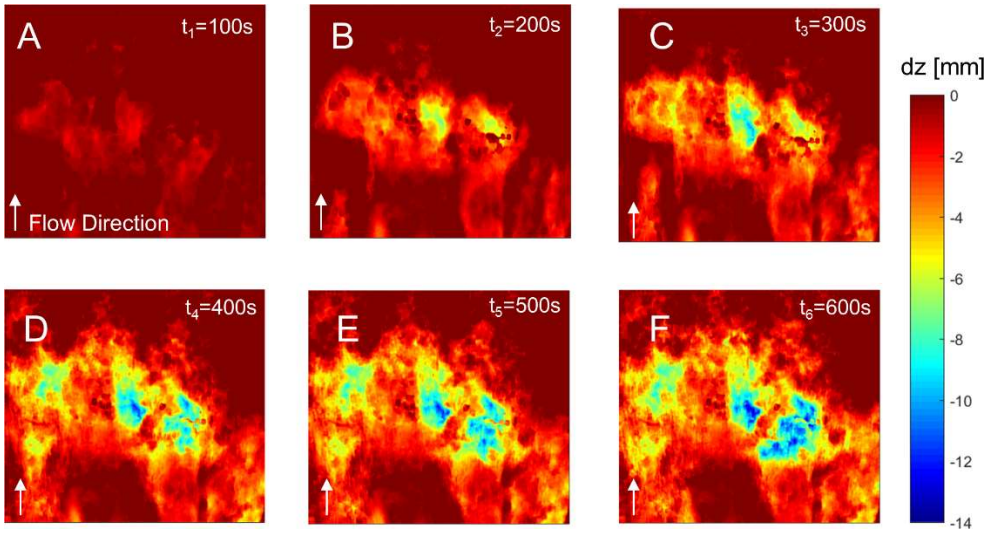

Figure 8. Temporal erosion progress of the erosion experiment with Q_2 = 11.3 L/s (*x*-*y*-plane) at six selected time-steps (Δt = 100 s).

Next to the variability of erosion rates, the visualized erosion progress in Figure 8A–F shows a continuously growing erosion pattern. The locations of initial erosion (Figure 8A) become larger and deeper over time (Figure 8B–F) indicating a relationship between erosion, surface roughness, and hydraulic forces. The local changes of the surface may lead to local peaks of turbulent fluctuations that result in different formations of erosion patterns. Although the selected time-step in Figure 8 is 100 s, the currently used CMOS-camera is capable for temporal resolutions up to 10 Hz, allowing for deeper analysis of the progressive erosion patterns of cohesive sediments, or non-cohesive/cohesive sediment mixtures.

4. Conclusions

A novel and high-resolution photogrammetric approach for the detection of erosion rates for cohesive sediments, or non-cohesive/cohesive sediment mixtures, has been introduced (PHOTOSED). The method allows for detailed insights in the erosion phenomena of both cohesive sediments and non-cohesive/cohesive sediment mixtures. The experimental setup uses a semiconductor laser with a diffraction optic to project a pseudo-random pattern of light points on a sediment surface, a CMOS-camera for image acquisition, and a dense optical flow (DOF) algorithm with the OpenCV library that evaluates the displacements of the light points of two consecutive images during the erosion process to assess the erosion volume. The calibration and verification procedure showed that the PHOTOSED method allows the detection of erosion volumes for several orders of magnitude with a minimum detection limit of approx. 15 mm^3 and enabling high-resolution measurements of erosion rates, as well as in-depth investigations of the erosion behavior of cohesive sediments and cohesive/non-cohesive sediment mixtures. One limitation is the shading of projected light points in cases of instantaneous and severe erosion depths with nearly vertical gradients given to the angled mounting of the semiconductor laser. However, the DOF algorithm returns an erosion volume based on two consecutive images for a selected time interval. This erosion volume and thus the occurred erosion depth can be subdivided into intermediate erosion stages by shortening the time interval between these two consecutive images given the high temporal resolution of the CMOS-camera (10 Hz).

The PHOTOSED method was subsequently applied to a sediment surface consisting of a cohesive/non-cohesive sediment mixture at two different flow rates. The results identify a high variability of the erosion rates within time intervals of 30 s and variability factors up to 10 between the median erosion rate and the maximum erosion rate. The high variability of erosion rates distributed over the entire sediment surface emphasizes the need to study the erosion phenomena of cohesive

sediments, or cohesive/non-cohesive sediment mixtures, in detail using high-resolution measurements. Although the sediment characteristics can significantly influence the dimensions of erosion rates, they are not limiting the accuracy of PHOTOSED because the method is based on the detection of erosion volumes, which also represents an advantage compared to devices working with suspended load measurements for the detection of erosion rates. However, if the erosion rates are related to hydraulic forces in form of shear stresses, the overall erosion pattern should not be too pronounced because of the influence of changing roughness on local hydraulics.

The high spatial and temporal resolution of PHOTOSED allows for the detection of different erosion patterns providing a high potential for further research including e.g., detailed studies of the interactions at the water-sediment interface or the unraveling of the complex interactions of physical, chemical and biological variables that are involved in determining the erosion stability. In addition, many practical issues in terms of sediment management in rivers, navigation channels, harbors or reservoirs can be addressed.

Author Contributions: The manuscript was written by M.N. with support of all co-authors. G.S. wrote the Python-Script to apply the DOF algorithm and did the calibration and verification experiments. F.B. and S.H. contributed by analyzing the spatial and temporal variability of the erosion processes. S.W. reviewed and edited the manuscript.

Acknowledgments: The authors gratefully acknowledge the assistance of undergraduate research assistants for their support during field measurements and data analyses. In addition, the authors express their sincere thanks to Caleb Inskeep for reviewing the script and language editing. The authors also gratefully acknowledge the financial support from the Water and Shipping Authority in Freiburg (WSA Freiburg), the German Federal Institute for Hydrology, and the Ministry of Science, Research and Arts in Baden-Württemberg, Germany. We also would like to acknowledge the anonymous reviewers for the valuable feedbacks.

Conflicts of Interest: The authors declare no conflict of interest.

References

1. Mirtskhoulava, T.E. Scouring by flowing water of cohesive and noncohesive beds. *J. Hydraul. Res.* **1991**, *29*, 341–354. [CrossRef]
2. Kothyari, U.C.; Jain, R.K. Erosion characteristics of cohesive sediment mixtures. In *River Flow 2010: Proceedings of the 5th International Conference on Fluvial Hydraulics (Vol. 1); Braunschweig, Germany, 8–10 September 2010*; Bundesanstalt für Wasserbau: Karlsruhe, Germany, 2010.
3. Wu, W.; Perera, C.; Smith, J.; Sanchez, A. Critical shear stress for erosion of sand and mud mixtures. *J. Hydraul. Res.* **2017**, *56*, 1–15. [CrossRef]
4. Paterson, D.M.; Black, K.S. Water flow, sediment dynamics and benthic biology. *Adv. Ecol. Res.* **1999**, *29*, 155–196. [CrossRef]
5. Parchure, T.M.; Mehta, A.J. Erosion of Soft Cohesive Sediment Deposits. *J. Hydraul. Eng.* **1985**, *111*, 1308–1326. [CrossRef]
6. Mitchener, H.; Torfs, H. Erosion of mud/sand mixtures. *Coast. Eng.* **1996**, *29*, 1–25. [CrossRef]
7. Sanford, L.P.; Maa, J.P.-Y. A unified erosion formulation for fine sediments. *Mar. Geol.* **2001**, *179*, 9–23. [CrossRef]
8. Van Prooijen, B.C.; Winterwerp, J.C. A stochastic formulation for erosion of cohesive sediments. *J. Geophys. Res.* **2010**, *115*, C01005. [CrossRef]
9. Walder, J.S. Dimensionless erosion laws for cohesive sediment. *J. Hydraul. Eng.* **2015**, *142*. [CrossRef]
10. Zhu, Y.; Lu, J.; Liao, H.; Wang, J.; Fan, B.; Yao, S. Research on cohesive sediment erosion by flow: An overview. *Sci. China Ser. E Technol. Sci.* **2008**, *51*, 2001–2012. [CrossRef]
11. Berlamont, J.; Ockenden, M.; Toorman, E.; Winterwerp, J.C. The characterisation of cohesive sediment properties. *Coast. Eng.* **1993**, *21*, 105–128. [CrossRef]
12. Black, K.S.; Tolhurst, T.J.; Paterson, D.M.; Hagerthey, S.E. Working with natural cohesive sediments. *J. Hydraul. Eng.* **2002**, *128*, 2–8. [CrossRef]
13. Aberle, J.; Nikora, V.; Walters, R. Effects of bed material properties on cohesive sediment erosion. *Mar. Geol.* **2004**, *207*, 83–93. [CrossRef]

14. Gerbersdorf, S.U.; Jancke, T.; Westrich, B. Physico-chemical and biological sediment properties determining erosion resistance of contaminated riverine sediments—Temporal and vertical pattern at the lauffen reservoir/river neckar, Germany. *Limnol.-Ecol. Manag. Inland Waters* **2005**, *35*, 132–144. [CrossRef]
15. Grabowski, R.C.; Droppo, I.G.; Wharton, G. Erodibility of cohesive sediment: The importance of sediment properties. *Earth-Sci. Rev.* **2011**, *105*, 101–120. [CrossRef]
16. Mehta, A.J.; Partheniades, E. Resuspension of deposited cohesive sediment beds. *Coast. Eng. Proc.* **1982**, *1*, 1569–1588.
17. Aberle, J. Measurement techniques for the estimation of cohesive sediment erosion. In *Hydraul. Methods for Catastrophes: Floods, Droughts, Environmental Disasters*; Rowiński, P.M., Ed.; Publications of the Institute of Geophysics, Polish Academy of Sciences: Warsaw, Poland, 2008; Volume 406, pp. 5–20.
18. Maa, J.P.-Y.; Wright, L.D.; Lee, C.-H.; Shannon, T.W. VIMS sea carousel: A field instrument for studying sediment transport. *Mar. Geol.* **1993**, *115*, 271–287. [CrossRef]
19. Bale, A.J.; Widdows, J.; Harris, C.B.; Stephens, J.A. Measurements of the critical erosion threshold of surface sediments along the Tamar Estuary using a mini-annular flume. *Cont. Shelf Res.* **2006**, *26*, 1206–1216. [CrossRef]
20. McNeil, J.; Taylor, C.; Lick, W. Measurements of erosion of undisturbed bottom sediments with depth. *J. Hydraul. Eng.* **1996**, *122*, 316–324. [CrossRef]
21. Roberts, J.D.; Jepsen, R.A.; James, S.C. Measurements of sediment erosion and transport with the adjustable shear stress erosion and transport flume. *J. Hydraul. Eng.* **2003**, *129*, 862–871. [CrossRef]
22. Noack, M.; Gerbersdorf, S.U.; Hillebrand, G.; Wieprecht, S. Combining field and laboratory measurements to determine the erosion risk of cohesive sediments best. *Water* **2015**, *7*, 5061–5077. [CrossRef]
23. Wan, C.F.; Fell, R. Investigation of rate of erosion of soils in embankment dams. *J. Geotech. Geoenviron. Eng.* **2004**, *130*, 373–380. [CrossRef]
24. Gust, G.; Muller, V. Interfacial hydrodynamics and entrainment functions of currently used erosion devices. In *Cohesive Sediments*; Burt, N., Parker, R., Watts, J., Eds.; John Wiley & Sons, Ltd.: Chichester, UK, 1997; pp. 149–174.
25. Tolhurst, T.J.; Black, K.S.; Paterson, D.M.; Mitchener, H.J.; Termaat, G.R.; Shayler, S.A. A comparison and measurement standardisation of four in situ devices for determining the erosion shear stress of intertidal sediments. *Cont. Shelf Res.* **2000**, *20*, 1397–1418. [CrossRef]
26. Witt, O.; Westrich, B. Qunatification of erosion rates for undistrubed contaminated cohesive sediment cores by image analysis. *Hydrobiologia* **2003**, *494*, 271–276. [CrossRef]
27. Kern, U.; Haag, I.; Schürlein, V.; Holzwarth, M.; Westrich, B. Ein strömungskanal zur ermittlung der tiefenabhängigen erosionsstabilität von gewässersedimente. *Wasserwirtschaft* **1999**, *89*, 72–77.
28. Debnath, K.; Nikora, V.; Aberle, J.; Westrich, B.; Muste, M. Erosion of cohesive sediments resuspension, bed load, and erosion patterns from field experiments. *J. Hydraul. Eng.* **2007**, *133*, 508–520. [CrossRef]
29. Lucas, B.D.; Kanade, T. An iterative image registration technique with an application to stereo vision. In Proceedings of the 7th International Joint Conference on Artificial Intelligence, Vancouver, BC, Canada, 24–28 August 1981.
30. Farnebäck, G. Two-frame motion estimation based on polynomial expansion. In *Image Analysis*; Lecture Notes in Computer Science; Springer: Berlin, Heidelberg, 2003; pp. 363–370.
31. Noack, M.; Hillebrand, G.; Seidenkranz, U.; Wieprecht, S. Investigation on the erosion stability of cohesive sediment deposits in the weir channel of the barrage Iffezheim, river rhine. *Hydrol. Wasserbewirtsch.* **2016**, *60*, 164–175. [CrossRef]